# Noncontact phase-sensitive dynamic optical coherence elastography at megahertz rate

Manmohan Singh[1], Chen Wu[1], Chih-Hao Liu[1], Jiasong Li[1], Alexander Schill[1], Achuth Nair[1], Yury V. Kistenev[2], and Kirill V. Larin[1,2,3,*]

[1]Department of Biomedical Engineering, University of Houston
[2]Interdisciplinary Laboratory of Biophotonics, Tomsk State University, Tomsk 634050, Russia
[3]Department of Molecular Physiology and Biophysics, Baylor College of Medicine
*Address all correspondence to: Kirill V. Larin, University of Houston, Department of
Biomedical Engineering, 4800 Calhoun Road, Houston, Texas 77004.
Tel: (832)842-8834; Fax: (713)743-0226; E-mail: klarin@central.uh.edu

## ABSTRACT

Dynamic optical coherence elastography (OCE) techniques have shown great promise at quantitatively obtaining the biomechanical properties of tissue. However, the majority of these techniques have required multiple temporal OCT acquisitions (M-B mode) and corresponding excitations, which lead to clinically unfeasible acquisition times and potential tissue damage. Furthermore, the large data sets and extended laser exposures hinder their translation to the clinic, where patient discomfort and safety are critical criteria. In this work we demonstrate noncontact true kilohertz frame-rate dynamic optical coherence elastography by directly imaging a focused air-pulse induced elastic wave with a home-built phase-sensitive OCE system based on a 4X buffered Fourier Domain Mode Locked swept source laser with an A-scan rate of ~1.5 MHz. The elastic wave was imaged at a frame rate of ~7.3 kHz using only a single excitation. In contrast to previous techniques, successive B-scans were acquired over the measurement region (B-M mode) in this work. The feasibility of this method was validated by quantifying the elasticity of tissue-mimicking agar phantoms as well as porcine corneas *ex vivo* at different intraocular pressures. The results demonstrate that this method can acquire a depth-resolved elastogram in milliseconds. The reduced data set enabled a rapid elasticity assessment, and the ultra-fast acquisition speed allowed for a clinically safe laser exposure to the cornea.

**Keywords:** Optical coherence elastography, cornea, Fourier domain mode-locked

## 1. INTRODUCTION

The biomechanical properties of tissues can provide critical information for detection of diseases. For example, keratoconus structurally degenerates the cornea, leading to significant reduction of visual quality or even complete blindness [1]. Other diseases, such as atherosclerosis [2], fibrosis [3], and cancer [4], can also alter biomechanical properties of tissues. Hence, physicians have been utilizing manual palpation as a technique to detect malignancies. However, manual palpation is subject and a quantitative technique would provide an objective basis for detecting diseases by changes in tissue biomechanical properties.

Therefore, various elastographic techniques have been developed to image mechanical contrast in tissues. Ultrasound elastography (USE) [5] and magnetic resonance elastography (MRE) [6] are valuable clinical techniques for detecting diseases such as breast cancer [7] and hepatic fibrosis [3]. These techniques rely on externally induced deformations, which are then detected by the parent imaging modality. However, USE and MRE require relatively large displacement

amplitudes and cannot provide micrometer-scale spatial resolutions, both of which inhibit their use for small and thin samples, such as the cornea.

The Ocular Response Analyzer and CorVis are two commercially available products capable of evaluating corneal biomechanical properties [8, 9]. Both devices measure the corneal response to a large amplitude air-puff. However, the large amplitude of the deformation (millimeter scale) induces a nonlinear response and subsequent nonlinear measurement, which is then used to characterize corneal biomechanical properties. Although some investigations have shown that the ORA can measure the onset and severity of disease [8], others have shown that the ORA cannot correctly detect eyes suspect of keratoconus [10]. Furthermore, the CorVis showed no difference in eyes before and after collagen cross-linking [11]. Brillouin microscopy can map the Brillouin shift in tissue with micrometer-scale spatial resolution with no external excitation. However, accurately quantifying Young's modulus from the Brillouin shift is still a challenge [12].

The elastographic functional extension of optical coherence tomography (OCT) [13], termed optical coherence elastography (OCE), is an emerging technique which utilizes the superior spatial resolution of OCT as compared to USE and MRE [14, 15]. By analyzing the phase of the complex OCT signal, displacement sensitivity can reach the nanometer scale [16]. This enables the use of minimal force, ensuring the preservation of the structure and function of delicate tissues such as the cornea. The advantages of OCE have been demonstrated for characterizing the elasticity of bioengineered tissue [17], tissue margin detection [18], and assessing the depth-resolved micrometer-scale elasticity of the cornea [19]. Combining OCE with a noncontact stimulus method such as an air-pulse allows for a noninvasive method of characterizing the elasticity of a sample [20].

The development of Fourier domain mode-locked (FDML) swept source lasers [21, 22] has enabled ultra-fast OCT imaging, which when combined with graphics processing unit (GPU) accelerated software [23], has enabled real-time video-rate OCT imaging [24, 25].

OCE has been able to reach kilohertz equivalent frame rates by synchronizing stimulations with M-mode images [26, 27]. We have previously developed a noncontact dynamic OCE technique called shear-wave imaging OCE (SWI-OCE) to assess the elasticity of hyaline cartilage [28], cardiac muscle [29], soft tissue tumors [30], and the cornea [31] by analyzing various parameters of an air-pulse induced elastic wave. While we were able to achieve an equivalent kilohertz frame-rate (equal to the A-scan rate of the system), this technique required multiple excitations and M-mode acquisitions for a single measurement. This led to clinically unfeasible acquisition times of a few minutes, which also resulted in exceeding the MPE limit for most tissues. In this work, we report a noncontact phase-sensitive OCE technique with a true kilohertz frame-rate by directly imaging the propagation of an air-pulse induced elastic wave. A single focused air-pulse induced low amplitude (micrometer-scale) elastic waves in tissue-mimicking agar phantoms of various concentrations. The elasticity was quantified by translating the group velocity to Young's modulus. The results were in reasonable agreement with the stiffness as obtained by uniaxial mechanical compression testing, demonstrating the feasibility of this technique. After these pilot experiments, this technique was tested on an *in situ* porcine cornea in the whole eye-globe configuration at various intraocular pressures (IOP).

## 2.   MATERIALS AND METHODS

Tissue-mimicking agar phantoms of various concentrations (1%, 1.5%, and 2%, w/w, n=3 for each concentration) were cast as samples of varying elasticities. To increase scattering in the near infrared, ink was added.

The home-built phase-sensitive optical coherence elastography (PhS-OCE) system was a combination of a ~7.3 kHz resonant scanner (Electro-Optical Products Corp., NY, USA), phase-sensitive optical coherence tomography (PhS-OCT) system, and a focused air-pulse delivery device. A schematic of the experimental setup is shown in Fig. 1. The PhS-OCT system was comprised of an FDML swept source laser (OptoRes Gmbh, Munich, Germany) with an A-scan rate of ~1.5 MHz, central wavelength of 1316 nm, scan range of 100 nm, and output power of up to 160 mW. The axial resolution of the system was ~16 μm, the sensitivity of the system was 106 dB, and the phase stability was ~14 nm in air. The air-

pulse device consisted of an arbitrary waveform generator that output a 2 ms wide square pulse to a voltage amplifier, which in turn powered an electronically-controlled pneumatic solenoid. The waveform generator was synchronized with the acquisition trigger of the PhS-OCE system to ensure proper synchronization and acquisition of the elastic wave. The air-port tip was kept ~250 μm from the surface of the sample and had a flat edge and inner diameter of ~150 μm.

A focused air-pulse induced a low amplitude deformation (μm scale) in the sample, which then propagated as an elastic wave [32]. The elastic wave was then directly imaged by continuously acquiring B-scans (B-M-mode) in a ~4 mm line along the elastic wave propagation path for ~30 ms. Only the linear region of the scan was utilized, and only the forward scan was utilized to eliminate scanning hysteresis artifacts. Immediately after the OCE measurements, the stiffness of the phantoms was assessed by uniaxial mechanical testing (Model 5943, Instron Corp., MA, USA) [33].



Figure 1. Schematic of experimental system. ADC: Analog-to-digital converter. DAC: Digital-to-analog converter.

The phase data was masked from the intensity image to remove the influence of poorly scattering pixels. The intensity image was used to identify the surface of the sample for motion and refractive index compensation [34]. The temporal vertical displacement profiles at the surface, $d_{surface}(t)$, were translated from the raw unwrapped surface vertical temporal phase profiles, $\varphi_{surface}(t)$, by:

$$d_{surface}(t) = \frac{\lambda_0}{4\pi n_{air}} \times \varphi_{surface}(t) \,, \tag{1}$$

and the displacement profiles inside the sample, $d_{inside}(t)$, were calculated from the phase profiles inside the sample, $\varphi_{inside}(t)$, by:

$$d_{inside}(t) = \frac{\lambda_0}{4\pi n_{sample}} \times \left[ \varphi_{inside}(t) + \varphi_{surface}(t) \times \left( n_{sample} - n_{air} \right) \right] . \tag{2}$$

The phase profiles were obtained from the phase differences between successive B-scans [26].

The elastic wave group velocity was determined by cross-correlation analysis. For each imaged in-depth layer, cross-correlation was performed between a reference position near the excitation and each transverse measurement position (n=75). The resulting temporal elastic wave propagation delays were then linearly fitted to the corresponding measurement distances, and the velocity was obtained from the slope of the fit [28, 29]. This process was repeated for

each imaged in-depth layer to obtain the group velocity as a function of depth. The velocities were then averaged depth-wise, and the Young's modulus was quantified by the surface wave equation from the group velocity, $c_g$, by [30, 32]:

$$E = \frac{2\rho(1+\nu)^3}{(0.87+1.12\nu)^2} c_g^2,$$

(3)

where $\rho$=1000 kg/m$^3$ was the sample material density and $\nu$=0.49 was the Poisson's ratio to account for the nearly incompressible nature of the samples.

Because the acquisition time was a few dozen milliseconds, 10 measurements were taken over different areas of each phantom (but still centrally located), and the results were averaged sample-wise.

After the preliminary experiments on the agar phantoms, the elasticity of an *in situ* porcine corneal sample was measured as function of intraocular pressure (IOP). A whole fresh juvenile eye (J&J Packing Corp., TX, USA) was placed in a home built holder. The eye globe was cannulated with two 23G needles for artificial IOP control [35]. Here, 3 measurements were taken for each IOP (10, 15, and 20 mmHg) over the same region and the elasticity was quantified by Equation (2) as well with $\rho$=1062 kg/m$^3$ for the cornea [36].

## 3. RESULTS

Figure 2 shows the propagation of the air-pulse induced elastic wave in the agar phantoms at ~1.2 ms after excitation. Clearly, the elastic wave propagates faster as the agar concentration (and stiffness) increases.
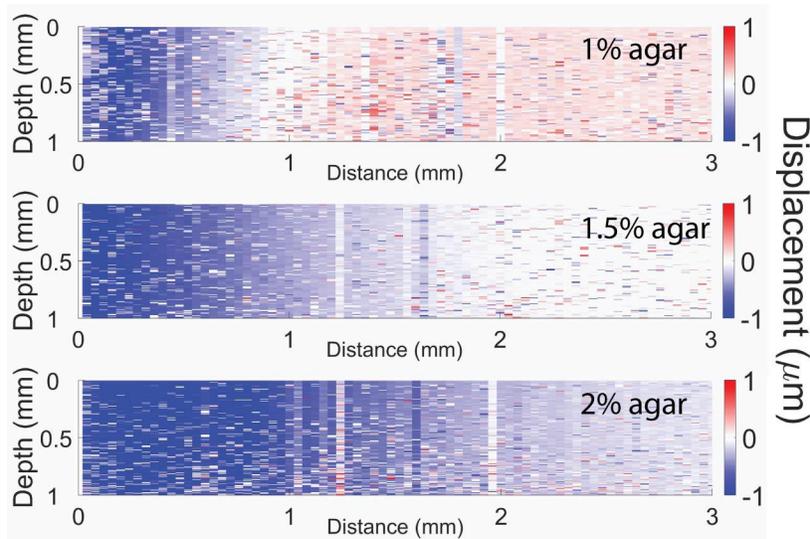


Figure 2: Air-pulse induced elastic wave propagation at 1.2 ms after excitation in agar phantoms of various concentrations.

Figure 3(a) shows the depth-wise group velocities from typical samples of each concentration. Figure 3(b) shows the comparison of the elasticity of the agar phantoms of various concentrations as estimated by OCE using Equation (3) compared to the stiffness as measured by mechanical testing (MT). The Young's moduli of the 1% phantoms were 11.0±0.6 kPa and 11.0 ±0.7 kPa as assessed by OCE and MT, respectively. For the 1.5% phantoms, the stiffness was 27.2±1.0 kPa as estimated by OCE and 17.6±4.4 kPa as measured by MT. The Young's modulus of the 2% phantoms was 60.9±7.3 kPa as quantified by OCE and 55.1±15.8 kPa as assessed by MT. As expected, stiffness increased along with agar concentration.
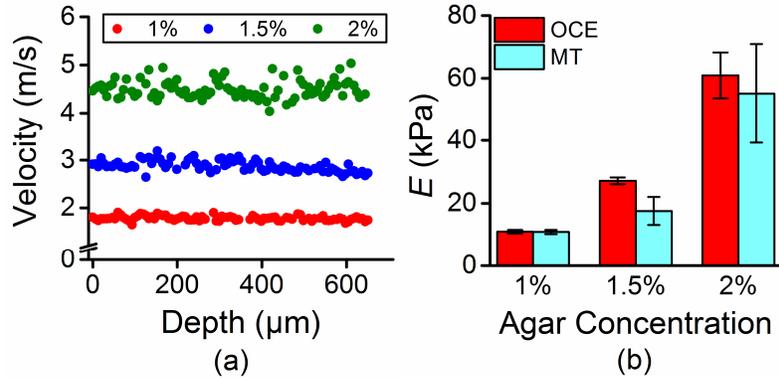
Figure 3: (a) Depth-wise group velocity of the air-pulse induced elastic wave in a typical sample from each concentration. (b) Young's modulus, *E*, of the phantoms of various concentrations as assessed by OCE using Equation (2) and as measured by uniaxial mechanical compression testing (MT).

Figure 4 plots the elasticity of the *in situ* porcine cornea at various IOPs as quantified by OCE utilizing Equation (2). The Young's modulus of the porcine cornea was estimated as 2.1±0.1 kPa, 4.9±1.0 kPa, and 15.7±5.1 kPa at 10, 15, and 20 mmHg IOP, respectively.
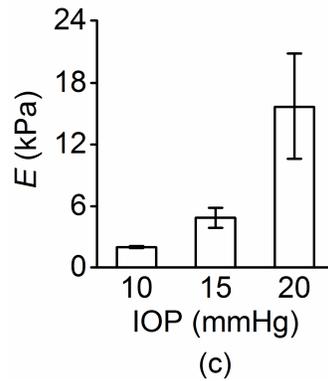


Figure 4: Young's modulus, *E*, of an *in situ* porcine cornea at various IOPs as assessed by OCE using Equation (3).

## 4. DISCUSSION

The elasticity of the phantoms and cornea was quantified using the surface wave equation (3). While it can provide a reasonable first order elasticity estimate [33], the surface wave equation cannot accurately replicate the true nature of the elastic wave, particularly in the cornea. Additionally, both the agar phantoms and cornea exhibit a non-linear stress-strain curve [33, 37], making accurate elasticity measurements difficult as obtaining the true strain encountered during the air-pulse OCE measurements is still a challenge. Nevertheless, the OCE technique demonstrated in this work allows for reasonable elasticity estimates as compared to MT. The corneal OCE results corroborate with previous OCE findings in the porcine cornea at similar conditions [38] and fall within the elasticity range reported in the literature under various conditions and with different measurement techniques [39-41].

Shear wave OCE at a true kilohertz frame-rate has been previously demonstrated using a 2D full-field OCT system with four-step phase shifting [42]. However, the sample must be translated to obtain information from different depths,

whereas the presented technique could be combined with spectral analysis to obtain depth-resolved elasticity information [19], albeit with fewer spatial pixels but at a similar frame-rate.

The relatively large variance in the corneal results at 20 mmHg is mainly due to the limited number of spatial and temporal pixels available for quantifying the group velocity. There is an intrinsic trade-off between spatial and temporal resolution as more lateral pixels would result in a lower frame-rate, but this technique was still able to quantify the Young's modulus at an ultra-high frame-rate. The frame-rate in the presented technique could be doubled by utilizing both directions of the scanner, and more spatial pixels could be utilized by spatially re-sampling the data after proper calibration rather than utilizing only the linear scan region. Incorporating both of these improvements is currently in progress. Due to the single excitation and very brief acquisition time, the ANSI Z136.1 MPE limit for the cornea was not exceeded. Additionally, this technique was able to perform a single measurement and post-processing in under 5 minutes, which could be reduced to near real-time with GPU accelerated OCE [43].

## 5. CONCLUSIONS

We have shown a noncontact true kilohertz frame-rate phase-sensitive OCE technique. The feasibility of this technique was first demonstrated on tissue-mimicking agar phantoms of various concentrations and the results corroborated with uniaxial mechanical testing. The elasticity of an *in situ* porcine cornea in the whole eye-globe configuration was then tested at various artificially controlled IOPs, and the results show that the elasticity of the cornea increases as a function of IOP.

## ACKNOWLEDGEMENTS

## REFERENCES

[1]     M. C. Chirambo, and D. Benezra, "Causes of blindness among students in blind school institutions in a developing country," British journal of ophthalmology, 60(9), 665-668 (1976).

[2]     N. M. van Popele, D. E. Grobbee, M. L. Bots et al., "Association between arterial stiffness and atherosclerosis The Rotterdam Study," Stroke, 32(2), 454-460 (2001).

[3]     M. Yin, J. A. Talwalkar, K. J. Glaser et al., "Assessment of hepatic fibrosis with magnetic resonance elastography," Clin Gastroenterol Hepatol, 5(10), 1207-1213 (2007).

[4]     A. Lyshchik, T. Higashi, R. Asato et al., "Thyroid gland tumor diagnosis at US elastography 1," Radiology, 237(1), 202-211 (2005).

[5]     J. Ophir, I. Cespedes, H. Ponnekanti et al., "Elastography: a quantitative method for imaging the elasticity of biological tissues," Ultrason Imaging, 13(2), 111-34 (1991).

[6]     R. Muthupillai, D. J. Lomas, P. J. Rossman et al., "Magnetic resonance elastography by direct visualization of propagating acoustic strain waves," Science, 269(5232), 1854-7 (1995).

[7]     A. Itoh, E. Ueno, E. Tohno et al., "Breast disease: clinical application of US elastography for diagnosis," Radiology, 239(2), 341-50 (2006).

[8]     D. P. Pinero, J. L. Alio, R. I. Barraquer et al., "Corneal biomechanics, refraction, and corneal aberrometry in keratoconus: an integrated study," Invest Ophthalmol Vis Sci, 51(4), 1948-55 (2010).

[9]     B. Valbon, R. Ambrósio Jr, B. Fontes et al., "Ocular Biomechanical Metrics by CorVis ST in Healthy Brazilian Patients," Journal of refractive surgery (Thorofare, NJ: 1995), 1-6 (2014).

[10]    A. Saad, Y. Lteif, E. Azan *et al.*, "Biomechanical properties of keratoconus suspect eyes," Investigative ophthalmology & visual science, 51(6), 2912-2916 (2010).

[11]    D. S. Grewal, G. S. Brar, R. Jain *et al.*, "Corneal collagen crosslinking using riboflavin and ultraviolet-A light for keratoconus: one-year analysis using Scheimpflug imaging," J Cataract Refract Surg, 35(3), 425-32 (2009).

[12]    G. Scarcelli, S. Besner, R. Pineda *et al.*, "Biomechanical characterization of keratoconus corneas ex vivo with Brillouin microscopy," Investigative ophthalmology & visual science, IOVS-14-14450 (2014).

[13]    D. Huang, E. A. Swanson, C. P. Lin *et al.*, "Optical coherence tomography," Science, 254(5035), 1178-81 (1991).

[14]    J. Schmitt, "OCT elastography: imaging microscopic deformation and strain of tissue," Opt Express, 3(6), 199-211 (1998).

[15]    B. F. Kennedy, K. M. Kennedy, and D. D. Sampson, "A review of optical coherence elastography: fundamentals, techniques and prospects," (2014).

[16]    M. Sticker, C. K. Hitzenberger, R. Leitgeb *et al.*, "Quantitative differential phase measurement and imaging in transparent and turbid media by optical coherence tomography," Optics Letters, 26(8), 518-520 (2001).

[17]    H. J. Ko, W. Tan, R. Stack *et al.*, "Optical coherence elastography of engineered and developing tissue," Tissue Eng, 12(1), 63-73 (2006).

[18]    K. M. Kennedy, B. F. Kennedy, R. A. McLaughlin *et al.*, "Needle optical coherence elastography for tissue boundary detection," Opt Lett, 37(12), 2310-2 (2012).

[19]    S. Wang, and K. V. Larin, "Noncontact depth-resolved micro-scale optical coherence elastography of the cornea," Biomed Opt Express, 5(11), 3807-21 (2014).

[20]    C. Dorronsoro, D. Pascual, P. Pérez-Merino *et al.*, "Dynamic OCT measurement of corneal deformation by an air puff in normal and cross-linked corneas," Biomedical optics express, 3(3), 473-487 (2012).

[21]    R. Huber, D. C. Adler, and J. G. Fujimoto, "Buffered Fourier domain mode locking: unidirectional swept laser sources for optical coherence tomography imaging at 370,000 lines/s," Opt Lett, 31(20), 2975-2977 (2006).

[22]    R. Huber, M. Wojtkowski, and J. G. Fujimoto, "Fourier Domain Mode Locking (FDML): A new laser operating regime and applications for optical coherence tomography," Opt Express, 14(8), 3225-37 (2006).

[23]    K. Zhang, and J. U. Kang, "Real-time 4D signal processing and visualization using graphics processing unit on a regular nonlinear-k Fourier-domain OCT system," Opt Express, 18(11), 11772-84 (2010).

[24]    T. Klein, W. Wieser, L. Reznicek *et al.*, "Multi-MHz retinal OCT," Biomed Opt Express, 4(10), 1890-908 (2013).

[25]    W. Drexler, M. Liu, A. Kumar *et al.*, "Optical coherence tomography today: speed, contrast, and multimodality," J Biomed Opt, 19(7), 071412 (2014).

[26]    S. Song, Z. Huang, T. M. Nguyen *et al.*, "Shear modulus imaging by direct visualization of propagating shear waves with phase-sensitive optical coherence tomography," J Biomed Opt, 18(12), 121509 (2013).

[27]    S. Wang, and K. V. Larin, "Shear wave imaging optical coherence tomography (SWI-OCT) for ocular tissue biomechanics," Opt Lett, 39(1), 41-4 (2014).

[28]    C. H. Liu, M. N. Skryabina, J. Li *et al.*, "Measurement of the temperature dependence of Young's modulus of cartilage by phase-sensitive optical coherence elastography," Quantum Electronics, 44(8), 751-756 (2014).

[29]    S. Wang, A. L. Lopez, 3rd, Y. Morikawa *et al.*, "Noncontact quantitative biomechanical characterization of cardiac muscle using shear wave imaging optical coherence tomography," Biomed Opt Express, 5(7), 1980-92 (2014).

[30]    S. Wang, J. S. Li, R. K. Manapuram *et al.*, "Noncontact measurement of elasticity for the detection of soft-tissue tumors using phase-sensitive optical coherence tomography combined with a focused air-puff system," Opt Lett, 37(24), 5184-5186 (2012).

[31]    Z. Han, S. R. Aglyamov, J. Li *et al.*, "Quantitative assessment of corneal viscoelasticity using optical coherence elastography and a modified Rayleigh-Lamb equation," J Biomed Opt, 20(2), 20501 (2015).

[32]    S. Wang, K. V. Larin, J. S. Li *et al.*, "A focused air-pulse system for optical-coherence-tomography-based measurements of tissue elasticity," Laser Phys Lett, 10(7), 075605 (2013).

[33]    Z. Han, J. Li, M. Singh *et al.*, "Quantitative methods for reconstructing tissue biomechanical properties in optical coherence elastography: a comparison study," Phys Med Biol, 60(9), 3531-47 (2015).

[34]     S. Song, Z. Huang, and R. K. Wang, "Tracking mechanical wave propagation within tissue using phase-sensitive optical coherence tomography: Motion artifact and its compensation," Journal of biomedical optics, 18(12), 121505-121505 (2013).

[35]     M. D. Twa, J. Li, S. Vantipalli et al., "Spatial characterization of corneal biomechanical properties with optical coherence elastography after UV cross-linking," Biomed Opt Express, 5(5), 1419-27 (2014).

[36]     J. Kampmeier, B. Radt, R. Birngruber et al., "Thermal and biomechanical parameters of porcine cornea," Cornea, 19(3), 355-363 (2000).

[37]     A. Elsheikh, and K. Anderson, "Comparative study of corneal strip extensometry and inflation tests," J R Soc Interface, 2(3), 177-85 (2005).

[38]     J. Li, Z. Han, M. Singh et al., "Differentiating untreated and cross-linked porcine corneas of the same measured stiffness with optical coherence elastography," J Biomed Opt, 19(11), 110502 (2014).

[39]     S. Kling, L. Remon, A. Perez-Escudero et al., "Corneal biomechanical changes after collagen cross-linking from porcine eye inflation experiments," Invest Ophthalmol Vis Sci, 51(8), 3961-8 (2010).

[40]     A. Elsheikh, D. Alhasso, and P. Rama, "Biomechanical properties of human and porcine corneas," Exp Eye Res, 86(5), 783-790 (2008).

[41]     E. Mikula, K. Hollman, D. Chai et al., "Measurement of corneal elasticity with an acoustic radiation force elasticity microscope," Ultrasound Med Biol, 40(7), 1671-1679 (2014).

[42]     A. Nahas, M. Tanter, T. M. Nguyen et al., "From supersonic shear wave imaging to full-field optical coherence shear wave elastography," J Biomed Opt, 18(12), 121514 (2013).

[43]     R. W. Kirk, B. F. Kennedy, D. D. Sampson et al., "Near Video-Rate Optical Coherence Elastography by Acceleration With a Graphics Processing Unit," J Lightwave Technol, 33(16), 3481-3485 (2015).